



**HAL**  
open science

## Multi-scale strategy for modeling macrocracks propagation in reinforced concrete structures

Christian Nader, Pierre Rossi, Jean-Louis Tailhan

► **To cite this version:**

Christian Nader, Pierre Rossi, Jean-Louis Tailhan. Multi-scale strategy for modeling macrocracks propagation in reinforced concrete structures. *Cement and Concrete Composites*, 2019, 99, pp.262 - 274. 10.1016/j.cemconcomp.2018.04.012 . hal-03484519v1

**HAL Id: hal-03484519**

**<https://hal.science/hal-03484519v1>**

Submitted on 20 Dec 2021 (v1), last revised 29 Mar 2022 (v2)

**HAL** is a multi-disciplinary open access archive for the deposit and dissemination of scientific research documents, whether they are published or not. The documents may come from teaching and research institutions in France or abroad, or from public or private research centers.

L'archive ouverte pluridisciplinaire **HAL**, est destinée au dépôt et à la diffusion de documents scientifiques de niveau recherche, publiés ou non, émanant des établissements d'enseignement et de recherche français ou étrangers, des laboratoires publics ou privés.



Distributed under a Creative Commons Attribution - NonCommercial 4.0 International License

# 1     **Multi-scale Strategy for Modeling Macrocracks Propagation in** 2     **Reinforced Concrete Structures**

3  
4     **Christian Nader, Pierre Rossi<sup>1</sup>, Jean-Louis Tailhan**

5  
6     Institut Français des Sciences et Technologies des Transports, de l'Aménagement et des  
7     Réseaux (IFSTTAR), Université Paris-Est

## 8 9 10 11 12    **Abstract**

13  
14    This paper introduces a new approach to model cracking processes in large reinforced  
15    concrete structures, like dams or nuclear power plants. For these types of structures it is  
16    unreasonable, due to calculation time, to explicitly model rebars and steel-concrete bonds. To  
17    solve this problem, we developed, in the framework of the finite element method, a  
18    probabilistic macroscopic cracking model based on a multi-scale simulation strategy: the  
19    Probabilistic Model for (finite) Elements of Reinforced Concrete (PMERC).

20    The PMERC's identification strategy is case-specific because it holds information about the  
21    local behaviour, obtained in advance via numerical experimentations.

22    The Numerical experimentations are performed using a validated cracking model allowing a  
23    fine description of the cracking processes.

---

<sup>1</sup>     **Corresponding author : Tel.:+ 33 6 80 01 72 26**  
      **E-mail address: pierre.rossi@ifsttar.fr (Pierre Rossi)**

24 The method used in the inverse analysis is inspired from *regression algorithms*: data on the  
25 local scale would shape the macroscopic model.

26 Although the identification phase can be relatively time-consuming, the structural simulation  
27 is as a result, very fast, leading to a sensitive reduction of the overall computational time.

28 A validation of this multi-scale modelling strategy is proposed. This validation concerns the  
29 analysis of the propagation of a macrocrack in a very large Double Cantilever Beam  
30 specimen (DCB specimen usually used in the framework of Fracture Mechanics studies)  
31 containing rebars. Promising results in terms of global behaviour, macrocracking information  
32 and important reduction in simulation time are obtained.

33

#### 34 **Keywords**

35

36 Reinforced concrete structures; Cracking process; Finite Elements; Multi-Scale Modelling  
37 Strategy; Probabilistic Approach.

38

## 39 **1. Introduction**

40

41

42 IFSTTAR, the French Institute of Science and Technology for Transports, Development and  
43 Networks, has been developing a probabilistic explicit cracking model since 1987 [1]. The  
44 numerical model, originally developed to analyze the cracking of concrete, was more recently  
45 enhanced to explicitly take into account the presence of rebars and the bond between rebars  
46 and concrete (to model real concrete structures) [2 – 4].

47 The use of this type of numerical models constitutes a local modelling strategy. They are  
48 interesting because they yield reliable and precise information about the cracking process.  
49 They can also be used in the framework of numerical experimentations in case there is a lack  
50 of experimental data.

51 Nevertheless, the modelling level they consider becomes inefficient (due to the unreasonably  
52 high computational time) when the structures concerned are large or contain a high  
53 percentage of rebars, which is the case for almost all complex real-life structures such as  
54 dams or nuclear power plants.

55 Nowadays, there exist other techniques to model cracking in large structures [5 - 8]. They are  
56 mainly based on homogenization approach of reinforced concrete. Although these techniques  
57 are interesting, they presents two main limitations: they do not give precise information about  
58 macrocracks opening and they remain relatively computational time consuming(when large  
59 reinforced structures are concerned).

60 The objective of this work is to propose a more relevant solution which allows (for design  
61 offices) to obtain good information about the macrocracking (macrocracks spacing and  
62 opening) of a large reinforced concrete structure in a reasonable computational time.

63 This solution is the Probabilistic macroscopic Model for finite Elements of Reinforced  
64 Concrete (PMERC).

65 The strategy of development of this 3D numerical model its theoretical formulation and its  
66 validation are presented, in detail, in this paper.

67

68

## 69 **2. Strategy for developing a PMERC**

70

71

72 The strategy has been broken down into distinct steps that map different scales of modelling.

73 The model depends on the dimensions and the configuration of the macro element (total

74 section and number of rebars taken into account in each macro element, for example) which

75 depend on the boundary conditions of the structural problem. The PMERC is thought in terms

76 of its two interconnected components: the macro element itself (the ERC part of the PMERC

77 acronym) defined by its dimensions and configuration, and the probabilistic model (the PM

78 part of the PMERC acronym) describing its behaviour.

79 A strong assumption is therefore made, which states that the ERC behaves only in tension in

80 the considered direction(s) of reinforcement(s). To be more precise, it is assumed that only

81 one macrocrack appears in each macro element, this macrocrack being oriented

82 perpendicularly to the rebar direction.

83 The Multi-Scale Modelling Strategy can be summarized as follow:

84

85

86

87 **First step: determination of the fineness of the finite element mesh and of the dimension**  
88 **of the ERC(s)**

89 An elastic simulation of the given structure is performed taking into account the boundary  
90 conditions of our problem. 2D or 3D (as required) volume elements are used without  
91 describing any reinforcements. This step is necessary to determine the coarsest finite element  
92 mesh that would still yield the correct kinematic field. This will set an upper limit on the size  
93 of the macro elements. Subsequently, the fineness of the mesh and the optimal ERC(s)  
94 (optimal in terms of geometry, size, and ubiquity) are chosen.

95

96 **Second step: determination of the different tie-beams geometry**

97 One or multiple ERC(s) are now defined – distinct either by their dimensions and/or their  
98 composition (position, number, and type of rebars).

99 Different tie-beam numerical tests, for each ERC, in every direction of reinforcements  
100 (numerical experimentation phase) are then defined. The length of these tie-beam specimens  
101 has to be sufficient to get a representative cracking pattern (it means a cracking pattern which  
102 results in a correct way the number of macrocracks per length of tie-beam).

103

104 **Third step: numerical simulations of the different tie-beams by using a local modelling**  
105 **approach**

106 Numerical simulations on the tie-beams are run to get information about cracking and global  
107 responses. To that end, validated local models are used: a probabilistic explicit cracking  
108 model for concrete and an interface element model for steel-concrete bond (section 4).

109

110

111

112 **Fourth step: determination of the macroscopic model parameters of the different ERCs**

113 Results from the tie-beam simulations (along with some working knowledge) help to deduce,  
114 by inverse analysis, the cracking behaviour of the different ERCs. The mechanical  
115 macroscopic model and the method used to determine the parameters of the constitutive law  
116 are detailed in section 3.

117

118 **Fifth step: numerical analysis of the reinforced structure with the macroscopic model**

119 Due to the fact that the macroscopic model used is a probabilistic one, it is important to  
120 perform several simulations (Monte-Carlo approach) to get information about the scattering  
121 related to the structural behaviour. By this way, it is then easy to perform safety analysis of  
122 this structure.

123

124 The so-called FE<sup>2</sup> methods were developed and used, in the past, by others researchers [9,  
125 10]. They are based on the hierarchical, bottom-up one-way coupled description of the  
126 material using the finite element methods in both scales and computational homogenization  
127 procedures at the low scale. The main differences between their work and this one can be  
128 summarized as follow:

- 129 • They treated only the problem of material behaviour and not that of reinforced  
130 concrete structures behaviour.
- 131 • They did not develop probabilistic approaches.
- 132 • They did not precisely treat the problem of cracks opening.

133

134

135

136

### 137 **3. PMERC theory**

138

139

140 The model is required to have the following features:

- 141 • The ability to get information on macro-cracks spacing and openings in a large reinforced  
142 concrete structure.
- 143 • A probabilistic modelling to allow for a statistical analysis of the structural behaviour via  
144 a Monte Carlo approach (reliability analysis of the structure).

145

#### 146 **3.1. Formulation of the model**

147

148 To achieve our objectives, and still save on calculation time, the model has to be simple.

149 Therefore, some strong assumptions are made:

- 150 • At the global structural scale, our scale of interest, the concrete part of the PMERC  
151 breaks in a brittle way. Therefore, the composite element is assumed to have an elastic  
152 brittle behaviour. Only failure criteria in tension and in shear are considered (the criterion  
153 for shear is only relevant when compressive stress fields are involved). These criteria are  
154 applied at the centre of gravity of the ERC. As for concrete alone, the values of the  
155 tensile and shear strengths of the ERC are considered as random values. At the difference  
156 of concrete alone, the distribution function chosen for the ERC is not a Weibull one but a  
157 lognormal one is (it is an arbitrary choice).
- 158 • Once the matrix is broken, the stresses in the element plunge to zero – a reasonable  
159 approximation at the scale of structural elements. Then, immediately after, the rebars  
160 intervene mechanically. This requires a new evaluation of the coefficients of the stiffness  
161 matrix of the ERC – in the direction parallel to the rebars. The new values of these



162 coefficients are associated with the stiffness of the rebars and the phenomenon of tension  
163 stiffening. They are considered as random values. It is to take into account the  
164 mechanical scattering related to the tension stiffening phenomenon. A lognormal  
165 distribution function is chosen arbitrary for these random values. As a matter of fact, a  
166 Weibull distribution function is not physically relevant for the post-cracking behavior of  
167 the ERC.

- 168 • The PMERC accounts for the plastic behaviour of the rebars in the studied direction:  
169 when the linear elastic strain limit of the steel is reached at the center of gravity of the  
170 ERC, its behaviour would be represented by an elasto-perfectly-plastic model. We chose,  
171 for simplicity, to simulate this behaviour with a damage model (permanent deformations  
172 due to the yield of the rebars are not considered). This simplification is only possible if  
173 monotonically increasing loadings are involved, which the case in this work.

174

175 As explained before, the macro-element is reinforced in only one direction. It can therefore be  
176 considered as an orthotropic material. A fixed orthogonal reference frame is locally placed  
177 with its direction 1 as the one of the reinforcement. Next, in agreement with homogenization  
178 techniques, it is considered that the element consists of a smeared orthotropic material. Thus  
179 the elastic 3D constitutive law is:

180

$$\sigma = H \cdot \varepsilon \quad (1)$$

181

182

$$\begin{bmatrix} \sigma_{11} \\ \sigma_{22} \\ \sigma_{33} \\ \sigma_{12} \\ \sigma_{13} \\ \sigma_{23} \end{bmatrix} = \frac{1}{\Delta} \begin{bmatrix} \frac{(1 - \nu_{23} \cdot \nu_{32})}{E_2 E_3} & \frac{(\nu_{21} - \nu_{31} \cdot \nu_{23})}{E_2 E_3} & \frac{(\nu_{31} - \nu_{21} \cdot \nu_{32})}{E_2 E_3} & 0 & 0 & 0 \\ \frac{(\nu_{12} - \nu_{13} \cdot \nu_{32})}{E_1 E_3} & (1 - \nu_{31} \cdot \nu_{13}) & \frac{(\nu_{32} - \nu_{31} \cdot \nu_{12})}{E_1 E_3} & 0 & 0 & 0 \\ \frac{(\nu_{13} - \nu_{12} \cdot \nu_{23})}{E_1 E_2} & \frac{(\nu_{23} - \nu_{13} \cdot \nu_{21})}{E_1 E_2} & (1 - \nu_{12} \cdot \nu_{21}) & 0 & 0 & 0 \\ \text{SYM} & & & G_{12} \cdot \Delta & 0 & 0 \\ & & & 0 & G_{13} \cdot \Delta & 0 \\ & & & 0 & 0 & G_{23} \cdot \Delta \end{bmatrix} \begin{bmatrix} \varepsilon_{11} \\ \varepsilon_{22} \\ \varepsilon_{33} \\ 2\varepsilon_{12} \\ 2\varepsilon_{13} \\ 2\varepsilon_{23} \end{bmatrix} \quad (2)$$

183

184

$$\Delta = \frac{E_1 E_2 E_3}{1 - \nu_{23} \cdot \nu_{32} - \nu_{31} \cdot \nu_{13} - \nu_{12} \cdot \nu_{21} - 2 \cdot \nu_{23} \cdot \nu_{31} \cdot \nu_{12}} \quad (3)$$

185

186 Assumptions are made concerning the elastic coefficients of the orthotropic stiffness matrix

187 **H:**

188 •  $E_1$ : Young modulus in the direction of the rebars; calculated as a result of the average  
189 Young modulus of both the concrete and the rebars according to the rule of mixtures  
190 (Voigt model).

191 •  $E_2 = E_3$ : Young modulus of the concrete (an approximation).

192 •  $\nu_{12} = \nu_{13} = \nu_{23} = \nu_{32}$ : Poisson's ratio of the concrete.

193 •  $\frac{\nu_{21}}{E_2} = \frac{\nu_{12}}{E_1}$ ;  $\frac{\nu_{31}}{E_3} = \frac{\nu_{13}}{E_1}$  (to ensure that **H** is symmetric).

194 •  $G_{23}$ : Shear modulus of plain concrete (an approximation)

195 •  $G_{12} = G_{13}$ : Shear modulus that takes into consideration the presence of the rebars in  
196 the volume of the element with respect to the rule of mixtures (Voigt model).

197

198 When failure criteria are applied in tension (Rankine) or in shear (Tresca) the failure limit is  
199 reached and the stresses are then immediately picked up by a reduced elastic matrix  
200 representing the remaining contribution of the steel bars with some residual action from the

201 surrounding concrete (in the form of friction). Some terms of the initial elastic constitutive  
 202 relation (1 and 2) are then affected by a reduction coefficient,  $\beta$ :

203

$$\boldsymbol{\sigma} = \mathbf{H}' \cdot \boldsymbol{\varepsilon} \quad (4)$$

$$\begin{bmatrix} \sigma_{11} \\ \sigma_{22} \\ \sigma_{33} \\ \sigma_{12} \\ \sigma_{13} \\ \sigma_{23} \end{bmatrix} = \frac{1}{\Delta} \begin{bmatrix} \beta \frac{(1 - \vartheta_{23} \cdot \vartheta_{32})}{E_2 E_3} & \beta \frac{(\vartheta_{21} - \vartheta_{31} \cdot \vartheta_{23})}{E_2 E_3} & \beta \frac{(\vartheta_{31} - \vartheta_{21} \cdot \vartheta_{32})}{E_2 E_3} & 0 & 0 & 0 \\ \beta \frac{(\vartheta_{12} - \vartheta_{13} \cdot \vartheta_{32})}{E_1 E_3} & (1 - \vartheta_{31} \cdot \vartheta_{13}) & (\vartheta_{32} - \vartheta_{31} \cdot \vartheta_{12}) & 0 & 0 & 0 \\ \beta \frac{(\vartheta_{13} - \vartheta_{12} \cdot \vartheta_{23})}{E_1 E_2} & \frac{(\vartheta_{23} - \vartheta_{13} \cdot \vartheta_{21})}{E_1 E_2} & \frac{(1 - \vartheta_{12} \cdot \vartheta_{21})}{E_1 E_2} & 0 & 0 & 0 \\ & & & G_{12} \cdot \Delta & 0 & 0 \\ & & & 0 & G_{13} \cdot \Delta & 0 \\ & & & 0 & 0 & G_{23} \cdot \Delta \end{bmatrix} \begin{bmatrix} \varepsilon_{11} \\ \varepsilon_{22} \\ \varepsilon_{33} \\ 2\varepsilon_{12} \\ 2\varepsilon_{13} \\ 2\varepsilon_{23} \end{bmatrix} \quad (5)$$

204

205  $\beta$  could also be viewed as an anisotropic damage variable. Actually, the whole process  
 206 involving the drop in stresses, and the contribution of steel until yielding, can be numerically  
 207 represented by a damage formulation:

208  $\sigma_r$  is the constraint value in direction 1 (that of the reinforcement) right after the drop  
 209 resulting from the failure criterion being reached.  $E'_1$  is the residual stiffness in direction 1.  $\sigma_r$   
 210 and  $E'_1$ , along with  $\sigma_t^{cri}$  (the tensile strength of the uncracked element) are the unknown  
 211 model parameters.

212 The drop from  $\sigma_t^{cri}$  to  $\sigma_r$  can be the result of an initial anisotropic damage constant  $D_{ini}^c$ ,

213 where:

$$D_{ini}^c = 1 - \frac{\sigma_r}{\varepsilon_{0_1} \cdot E_1} \quad (6)$$

214  $\varepsilon_{0_1}$  here is the state of strain in direction 1 after the brittle failure of the element. So we  
 215 assume that the cracking of the element has damaged it and we now have established a  
 216 damage variable  $D^c$  with a lower bound  $D_{ini}^c$ .

217 The stresses are then picked up by the reduced elastic matrix represented by  $E'_1 = \beta E_1 =$   
 218  $(1 - D^c)E_1$  (physically the steel bars with some residual friction from the surrounding  
 219 concrete).

220  $D^c$  is considered a state variable, thus its evolution has to verify the following conditions:

$$\begin{cases} \dot{D}^c \geq 0 \\ D^c = \max(D_0^c, D^c) \end{cases} \quad (7)$$

221

222 Where  $D_0$  is the initial damage state, and  $D$  is the actual damage state. The initial damage  
 223 threshold ( $D_{ini}$  in this case) is established when the failure criterion is reached in the direction  
 224 of the reinforcement. Once the element is declared as cracked (failure criteria reached) the  
 225 damage evolution is then given by the following relations:

$$\begin{cases} D^c(\tilde{\varepsilon}) = D_{ini}^c ; \tilde{\varepsilon} \leq \varepsilon_{0_1} \\ D^c(\tilde{\varepsilon}) = 1 - \frac{\sigma_r + E'_1(\tilde{\varepsilon} - \varepsilon_{0_1})}{E_1 \tilde{\varepsilon}} ; \varepsilon_{0_1} < \tilde{\varepsilon} \leq \frac{\sigma^p - \sigma_r}{E'_1} + \varepsilon_{0_1} \end{cases} \quad (8)$$

$$D_{max}^c = \text{constant value if } \tilde{\varepsilon} \geq \frac{\sigma^p - \sigma_r}{E'_1} + \varepsilon_{0_1}$$

226 Where  $\tilde{\varepsilon} = \langle \varepsilon_1 \rangle_+$  ( $\langle \cdot \rangle_+$  is the positive part of  $(\cdot)$ ). This behavior is held until the  
 227 (predetermined) yield limit of the steel is reached.

228 To represent the plastic behavior of the reinforcements all it is needed to do is to update the  
 229 damage model. Note that it is not saying that plasticity is the same as damage, it is just used  
 230 the convenience of the damage formulation to represent the plastic behavior of the macro-  
 231 element. Once the stresses in the element reach the yield limit of the steel, the behavior of the  
 232 element will be represented as follows:

233

$$\boldsymbol{\sigma} = (1 - D^p)\mathbf{H}' \cdot \boldsymbol{\varepsilon} \quad (9)$$

$$\dot{D}^p \geq 0$$

234

235 And the damage evolution is now given by:

$$D^p(\tilde{\varepsilon}) = 1 - \frac{\sigma^p - \sigma_r + E'_1 \varepsilon_{0_1}}{E'_1 \tilde{\varepsilon}}; \quad \tilde{\varepsilon} > \frac{\sigma^p - \sigma_r}{E'_1} + \varepsilon_{0_1} \quad (10)$$

236

237 At this stage, the model still carries two unknown parameters: the tensile strength of the  
 238 uncracked element  $\sigma_t^{cri}$ , and the residual stiffness in direction 1,  $E'_1 = \beta E_1$  (stiffness of the  
 239 elastic steel bars in this direction, plus friction with the cracked concrete matrix). Lognormal  
 240 distribution functions are assigned to both  $\sigma_t^{cri}$  and  $E'_1$ .

241 It can be noted that the mean shear strength is assumed to be equal to the half of the  
 242 compressive strength, and its standard deviation is equal to that of the tensile strength.

243 If the fourth step of the numerical strategy (see section 2) is considered, the resulting force-  
 244 displacement curve from the global approach has to be fitted to that of the local approach  
 245 (numerical experimentations) on the tie-beam tests. The best fit will determine the different  
 246 parameters for both distribution functions. Consequently, this classifies the methodology as  
 247 an optimization problem. The optimization tool most suited for the problem is the Response  
 248 Surface Method (RSM) [11]. RSM is a way to explore the effect of operating conditions (the  
 249 factors/parameters) on the response variable,  $y$ . In the present case,  $y$  is the surface area of the  
 250 complex polygon outlined by the real force/displacement curve and the fitted curve. To  
 251 calculate the surface area of this highly irregular and self-intersecting polygon the Bentley-  
 252 Ottmann algorithm [12] is used. As the unknown response surface of  $y$  is mapped out, the  
 253 process continues as close as possible towards an optimum (i.e. the minimum value of the  
 254 considered area), taking into account any constraints.

255 At the end of this step, the parameters that minimize  $y$  are the ones which are input into the  
256 model for the final calculations.

257 To summarize, the parameters involved in the process of creating the complete mechanical  
258 model for a given ERC (given concrete and reinforcements) are:

- 259 • The parameters of the probabilistic explicit or semi-explicit cracking model of the  
260 concrete.
- 261 • The values of  $C$  and  $\delta_t^{cri}$  for the interface elements (steel-concrete bond model) which  
262 allows us to perform the correct numerical simulations of the tie-beam test(s). The  
263 results from these numerical simulations constitute the starting point for fitting the  
264 values of the parameters of the ERC.
- 265 • The elastic orthotropic stiffness matrix of the ERC, assembled with the help of some  
266 intuitive hypotheses and the rule of mixtures.
- 267 • The parameters of the lognormal distribution function for the tensile strength of the  
268 chosen ERC (in the direction of rebars).  
269 The average value of the tensile strength of a given ERC is necessarily smaller than  
270 the one for the same volume of plain concrete; the presence of rebars introduces an  
271 extra level of heterogeneity (concentration of stresses around the rebars) that promotes  
272 fracture initiation.
- 273 • The parameters of the lognormal distribution function for the shear strength of the  
274 ERC. The mean value is equal to half the average compressive strength of the  
275 considered concrete. Its deviation is considered identical to that of the ERC's tensile  
276 strength.
- 277 • The parameters of the lognormal distribution function of the residual stiffness of the  
278 ERC after cracking.

279 Figure 4 summarizes the model's pre and post cracking behaviour in the direction of the  
280 rebars.

281

### 282 **3.2. Probabilistic cracking models**

283

284 The probabilistic model was first developed at IFSTTAR (formerly LCPC) by Rossi [1, 13]  
285 and more recently improved by Tailhan et al. [14]. It describes the behaviour of concrete via  
286 its two major characteristics: heterogeneity, and sensitivity to scale effects [15]. The physical  
287 basis of the model (presented in detail in [1, 13]) can be summarized as follow:

288 1) The heterogeneity of concrete is due to its composition. The local mechanical  
289 characteristics (tensile strength  $f_t$ , shear strength  $\tau_c$ ) are randomly distributed.

290 2) The scale effects are a consequence of the heterogeneity of the material. The mechanical  
291 response directly depends on the volume of material that is stressed.

292 3) The cracking process is controlled by defects in the cement paste, by the heterogeneity of  
293 the material, and by the development of tensile stress gradients.

294 4) The following points specify how the numerical model accounts for these physical  
295 evidences:

296 5) The model is developed in the framework of the finite element method, each element  
297 representing a given volume of (heterogeneous) material.

298 6) The tensile strength is distributed randomly on all elements of the mesh using a Weibull  
299 distribution function whose characteristics depend on the ratio: *volume of the finite*  
300 *element/volume of the largest aggregate*, and the compressive strength (as a good  
301 indicator of the quality of the cement paste). The volume of the finite element depends on  
302 the mesh, while the volume of the largest aggregate is a property of the concrete [1, 13,  
303 14].

304 The Weibull distribution function is the best to take into account the rupture in tension of  
305 a brittle and heterogeneous material as concrete.

306 7) The shear strength is also distributed randomly on all elements using a distribution  
307 function: (1) its mean value is independent of the mesh size and is assumed equal to the  
308 half of the average compressive strength of the concrete and (2) its deviation depends on  
309 the element's size, and is the same (for elements of same size) as that of the tensile  
310 strength.

311 8) Concerning the cracks representation, two approaches are proposed:

312 a) *First approach: explicit cracking*

313 The cracks are explicitly represented by non-linear interface elements of zero thickness.  
314 These elements connect volume elements representing un-cracked plain concrete. Failure  
315 criteria of Rankin in tension and Tresca in shear (to take into account cracks generated by  
316 compressive stresses [16]) are used. As far as tensile or shear stresses remain lower than their  
317 critical values, the interface element ensures the continuity of displacements between the  
318 nodes of the two neighboring volume elements. The material cell gathering these two volume  
319 elements and the interface element remains therefore elastic. Once one of the preceding  
320 failure criteria is reached, the interface element opens and an elementary crack is created. The  
321 tensile and shear strengths as well as the normal and tangential stiffness values, related to this  
322 interface element, become equal to zero [1, 13, 14]. In case of crack re-closure, the interface  
323 element recovers its normal stiffness and follows a classical Coulomb's law [16].

324 Note that in this modelling approach, the creation and the propagation of a crack is the result  
325 of the creation of elementary failure planes that randomly appear and can coalesce to form the  
326 macroscopic cracks (Figure 1).

327

328



329 *b) Second approach: semi-explicit cracking*

330 The cracks are modeled using linear volume elements. At the finite element scale, the  
331 energetic effect associated to the elementary cracking process is represented through a simple  
332 isotropic damage law with a single scalar parameter [17] (the model is presented in details in  
333 [18]). A probabilistic energetic regularization is also retained.

334 Without going into details of numerical implementation of the model, its main features can be  
335 summarized as follows:

- 336 • A bilinear stress–strain relationship is used to represent elementary cracking (Figure  
337 2). The elementary dissipative process (i.e. crack propagation inside the FE itself)  
338 starts when the major principal stress at a given Gauss point equals the material tensile  
339 strength. Dissipation is then driven by the positive part of the projection of the strain  
340 along the normal direction of the major principal stress. When the total energy  
341 available for the FE is dissipated, it is declared cracked and its elementary stiffness  
342 matrix is set to zero [18]. This allows avoiding stress-locking phenomena.
- 343 • The model is numerically implemented using a rotating crack approach [20, 21].  
344 During the dissipative phase, the stress is allowed to evolve according to any changes  
345 in the stress state in the material.
- 346 • Differently from smeared-cracking approaches [21-23], no additive decomposition is  
347 introduced in the constitutive law to distinguish between elastic deformation and crack  
348 contributions. An elementary crack is supposed to exist only after the condition the  
349 damage parameter equal 1 is achieved [18]. The elementary crack opening is then  
350 computed from the projection of the elementary displacements along the normal  
351 direction of the major principal stress.
- 352 • For sake of simplicity, crack re-closure is not explicitly treated. The model assumes  
353 that the dissipative process does not influence the elementary stiffness in compression.

354           So, for reclosed cracks, the elementary stiffness matrix in compression is completely  
355           recovered while the elementary tensile strength is set to zero.

356

357   The constitutive law of the model is completely defined by two parameters: the tensile  
358   strength and the volumetric density of dissipated energy. An energetic regularization  
359   technique allows computing the volumetric density of dissipated energy from the surface  
360   cracking energy by dividing this last energy by an elementary characteristic length [24]. This  
361   elementary characteristic length,  $l_e$ , is here computed from elementary volume,  $V_e$ , as  $l_e =$   
362    $V_e^{1/3}$ . More complex definitions are possible, depending on the FE shape and the order of  
363   interpolation of the displacement field. This choice can influence the predicted crack paths,  
364   however due to the probabilistic aspects of the model this effect is strongly reduced. The  
365   volumetric density of dissipated energy is defined element-by element according to spatially  
366   uncorrelated lognormal statistical law [25]. This choice of a lognormal statistical law is an  
367   arbitrary one (the use of a Weibull law is not relevant anymore as for the tensile strength  
368   distribution due to the fact that, in this approach, the rupture is no more considered as  
369   perfectly brittle). As for the tensile strength parameters, the standard deviation related to the  
370   volumetric density of dissipated energy depend on the elementary volume. In contrary, the  
371   mean value of the energy distribution is assumed independent of elementary volume. Its value  
372   is estimated as  $2\gamma$  where  $\gamma$  is the specific fracture energy per unit area (which is an intrinsic  
373   material parameter) according Griffith's theory [26].

374   Note that in this modelling approach, the creation and the propagation of a crack is the result  
375   of the creation of elementary holes that randomly appear and can coalesce to form the  
376   macroscopic cracks.

377   It is important to underline that:

- 378       • The first approach gives a more precise and relevant information about the cracking  
379       description and the cracking process but is a lot of more simulation time consuming  
380       than the second approach.
- 381       • Due to this problem of simulation time consuming, the second approach is  
382       recommended to perform 3D simulations.

383

### 384 **3.3. Concrete/steel bond model**

385

386 Two modelling approaches were introduced to model the concrete-rebar bond [2, 3, and 4]:

- 387       • The concrete-rebar bond is represented by interface elements. Their behaviour is  
388       described with a simple deterministic damage model with only two parameters,  
389       cohesion and slip (i.e. relative tangential displacement between steel and concrete).
- 390       • The notches/indentations are explicitly modeled along the whole length of the rebar  
391       with a perfect bond between concrete and rebar.

392

393 The first approach needs to have experimental information about this steel-concrete bond in  
394 order to perform inverse analysis for determining the values of the interface model  
395 parameters.

396 The second approach is used only when you have not any experimental information about this  
397 steel-concrete bond. It is more local than the first one but also more time consuming.

398

#### 399 *The interface element for modeling the steel-concrete bond*

400 Its role is to:

- 401 • Ensure the displacement continuity between the concrete and the steel before the slip  
402 of the interface and before the cracking of the concrete, thus ensuring the transfer of  
403 stresses between steel and concrete.
- 404 • Represent the macroscopic mechanical effect of the rebar at the ribs – which is not  
405 explicitly represented in the mesh.
- 406 • Simulate a local failure between steel and concrete along the rebar resulting from a  
407 loss of the local adhesion due to shear cracking.
- 408 • Simulate the local friction between the concrete and the steel after the interface  
409 failure.

410

411 The model is implemented in 2D and 3D [2, 3]. It considers the concrete-rebar bond as a  
412 material zone that progressively degrades in shear (the tensile failure is neglected). Prior to  
413 total failure, stresses are continuously transmitted through the interface.

414 The interface model is based on a damage model that maintains a constant level of stress  
415 when the critical shear has been reached (Figure 3). When the relative tangential  
416 displacement between the concrete and the rebar exceeds a critical value, the interface  
417 element is declared broken [27]. After failure, a Mohr-Coulomb type of friction behaviour is  
418 maintained.

419 The interface model is deterministic. This is a valid approximation because the cracking  
420 process around the rebar is governed by the presence of the ribs (rather than the heterogeneity  
421 of concrete) [28].

422 Only the values of the maximum shear stress, and of the tangential critical relative  
423 displacement, have to be determined. It is realized by performing a numerical inverse  
424 analysis, it means by fitting tie-beam test results obtained with the rebar and the concrete  
425 concerned [2, 4].

426 In the framework of the proposed numerical modelling strategy, only 2D interface elements  
427 are used. As a matter of fact, it should be unrealistic, due to computational time  
428 considerations, to perform 3D numerical analysis of tie-beam tests. This assumption that a 2D  
429 numerical analysis (plane stresses conditions) of a 3D tie-beam test is acceptable has been  
430 clearly justified and validated in previous works [2, 4]

431

432

#### 433 **4. Example of application of the Multi-Scale Modelling Strategy**

434

435

436 As validation example, a structural problem that has been previously studied by the authors  
437 has been chosen [29-31]. This structural problem concerns the analysis of the macrocrack  
438 propagation in a Double Cantilever Beam (DCB) concrete specimen. This type of specimen  
439 and study are very common in the framework of Linear Fracture Mechanics theory. The  
440 specificity of the specimen concerned by this paper is related to two points: the first one  
441 concerns the fact that the dimensions of the specimen are very (unusually) important (3.5  
442 meters length and 1.1 meters width) and the second concerns the fact that the specimen  
443 contains rebars along of the potential propagation of the macrocrack [29].

444 So, this structural problem is clearly related to the propagation of a macrocrack over a long  
445 distance and crossing rebars. It is an interesting case in relation with the spirit of the  
446 modelling strategy approach presented in this paper.

447 To make a comparison between the local approach performances with the macroscopic  
448 approach performances, it has also been decided to model the DCB specimen behaviour in the  
449 framework of the local approach. As, it is not reasonable (due to simulation time

450 considerations), to use a 3D approach to achieve this local modelling, a 2D approach is  
451 performed.

452

#### 453 **4.1. Some details about the validation test**

454

455 The dimensions of the specimen and the loading conditions related to the test are presented in  
456 Figure 5. The steel bars used were ribbed ones with 6 mm diameter. The distance between the  
457 rebars was 10 cm and the first rebar was located at 30 cm from the front tip of the notch  
458 (Figure 6).

459 Note that the specimen contained a narrowed section in its center part to force the propagation  
460 of the macrocrack along this reduced section (Figure 5). For the same reason and objective,  
461 prestressing cables were used and placed along the flanges of the specimen (Figure 5).

462

#### 463 **4.2. Numerical simulations**

464

##### 465 4.2.1. 3D macroscopic approach

466 The first step of the modelling strategy (section 2) is to choose the dimensions of the ERC  
467 (dimensions of the “macro-element”). These dimensions have to be relevant in respect to the  
468 achievement of a correct kinematic field.

469 In the case of the DCB specimen concerned by this study (figure 5), two points have to be  
470 noted:

- 471 • The first one is that the mesh has to be very fine at the front tip of the notch where only  
472 concrete is present (high stresses concentration).

- 473       • The second one concerns the part of the specimen where rebars are present. In this  
474       part, there are not stresses concentration due to the mechanical acting of the rebars. So,  
475       the finite elements can be much larger.
- 476       • To evaluate the influence of the dimension of the ERC chosen both on the relevancy of  
477       the numerical results (by comparison with the experimental result) and the  
478       computational time, it has been decided to consider 3 types of ERC dimensions:
- 479       - ERC1: Length (L): 10 cm, High (H): 10 cm, Thickness (T): 10 cm.  
480       - ERC2: L: 10 cm, H: 5 cm, T: 10 cm.  
481       - ERC3: L: 10 cm, H: 20 cm, T: 10 cm.

482

483   It can be noted that:

- 484       - ERC1 and ERC2 contain one rebar.  
485       - ERC3 contains two rebars.  
486       - The thickness of the 3 ERC is the same and equal to 10 cm, because it is assumed  
487       that the macrocrack will pass along the narrowed section of the DCB specimen. It  
488       means that, in this zone, only one ERC is present in the thickness of the DCB  
489       specimen

490

491   In Figure 7 is presented (as example) the 3D finite elements meshes containing, ERC1. In  
492   Figure 8 is presented 2D cuts of the three different 3D finite elements meshes (with ERC1,  
493   ERC2 and ERC3). It can be noted that for the finite element mesh related to the use of ERC2,  
494   it is necessary to introduce also finite elements representing only concrete.

495

496   The second step of the modelling strategy is related to the choice of the tie beam  
497   configurations (3 configurations, one by ERC), on which the inverse approach permitting to

498 determine the parameters of the macroscopic mechanical model associated to each ERC has  
499 to be performed. Considering Figure 7, the 3 tie-beams chosen for performing 2D (plane  
500 stresses conditions) simulations with the local approach have the following dimensions:

- 501 - ERC1: tie-beam 1 (TB1) with a high of 10 cm and a length of 140 cm.
- 502 - ERC2: TB2 with a high of 5 cm and a length of 140 cm.
- 503 - ERC3: TB3 with a high of 20 cm and a length of 140 cm.

504

505 The third step of the modeling strategy is, now, to perform the numerical simulations of the  
506 different tie-beams. Normally, to perform the numerical simulation in the framework of the  
507 local approach, the best way (related to computational time considerations, see section 4) to  
508 model the concrete/steel bond is to use interface elements.

509 The problem is that no tie-beam tests were performed in parallel to DCB test. So, it is not  
510 possible to determine the parameters of the interface element behaviour law.

511 The solution is to use the second way to model this steel-concrete bond (see section 4.2), it  
512 means to explicitly model all the notches/indentations of the rebars. Of course, this solution is  
513 computational time consuming, but it consists to replace experimental tests, which are also  
514 time consuming, by numerical tests.

515 The three 2D finite elements meshes related to the 3 numerical tie-beams (local approach and  
516 2D stresses plane conditions) are presented in Figure 9.

517 Concerning the probabilistic model used for the concrete, the semi-explicit approach is  
518 chosen (section 4.1).

519 Concerning the modeling of the rebars behaviour, a classical Von Mises law (perfect  
520 plasticity) is chosen.

521 The parameters values related to the concrete and the steel models are given in Table 1.



522 Figures 10, 11 and 12 present examples of cracking process obtained with the three numerical  
523 tie-beam tests.

524

525 The fourth step consists, now, to determine, by inverse approach, the parameters values  
526 related to the macroscopic model.

527 Figure 13 presents the three 3D finite elements meshes chosen to model the three tie-beams in  
528 the framework of the macroscopic approach.

529 Figures 14, 15 and 16 present the force-displacement curves obtained with the local and the  
530 macroscopic approaches respectively for the three tie-beams.

531 Table 2 gives the values of the material parameters used in the framework of the macroscopic  
532 model to get the results summarized by the Figures 14 to 16.

533

534 The fifth step of the modelling strategy consists, finally, to model the cracking behaviour and  
535 the global behaviour of the DCB specimen using the results obtained with the modelling of  
536 the three tie-beams.

537 The crack mouth opening displacement (CMOD) versus loading curves related to the three  
538 3D meshes are presented in Figures 17 to 19.

539 It can be noted that:

540 • As the macroscopic model is a probabilistic one, several numerical simulations are  
541 performed in relation with each 3D mesh.

542 • In each figure is reported the experimental curve (one test was performed [27])

543

544 An example of crack propagation using the macroscopic approach is presented in Figure 20.

545 To make a comparison between the local approach performances with the macroscopic  
546 approach performances, it has been decided to model the DCB specimen behaviour in the

547 framework of the local approach. As, it is not reasonable (due to simulation time  
548 considerations), to use a 3D approach to achieve this local modelling, a 2D approach is  
549 performed.

550

#### 551 4.2.2. 2D local approach

552 The first step of the 2D local approach is to determine the values of the parameters related to  
553 the concrete/steel bond model using interface elements (section 3.2). As a matter of fact, it is  
554 not still reasonable to perform the 2D modelling of the DCB specimen by representing the  
555 ribs of the rebars (as for the tie-beam).

556 To get these values, the way chosen is to perform an inverse approach (fitting approach) as  
557 proposed, realized and validated in [2-4]. To achieve this inverse approach, the 2D numerical  
558 simulations performed with the TB1 are considered as the reference results (Figures 7 and  
559 14).

560 The values of the parameters related to the concrete/steel bond model using interface  
561 elements are given in Table 3 (obtained from the inverse approach).

562 Figure 21 presents the 2D (plain stresses conditions) finite element mesh used to model the  
563 DCB specimen with the local approach.

564 Concrete is modeled by using the semi-explicit approach (see section 3.1).

565 The values of all the parameters involved in the numerical simulations (several numerical  
566 simulations are performed, the modelling of the concrete cracking being probabilistic) are  
567 those given in Tables 1 and 3.

568 Figure 22 presents the CMOD versus loading curves related to the numerical simulations. The  
569 experimental curve is also reported in the figure.

570 Figure 23 presents an example of cracking process obtained with the 2D local modelling.

571 It is now possible to analyze all the results obtained with all (2D and 3D) numerical  
572 simulations and to compare them.

573

### 574 **4.3. Analysis of the results and discussion**

575

576 This analysis and discussion is based on Figures 17 to 20 and 22 to 23.

577 A look of these figures leads to the following comments:

- 578 • The macroscopic approach (with the three different macro-elements) gives good  
579 enough results in terms of global behaviour of the DCB specimen (in comparison with  
580 the experimental result). It can be noted, however, that larger are the macro-elements,  
581 larger is the difference between the experimental result and the numerical simulations  
582 ones. It is an expected result. As a matter of fact, the numerical homogenization,  
583 linked to the numerical strategy of modelling proposed in this work, has to lead to a  
584 lost of precision of the information obtained (it is the price to pay).
- 585 • The local approach leads to a more scattered global behaviour of the DCB specimen  
586 than the macroscopic approach.. It is still a normal and expected result. As a matter of  
587 fact, the numerical homogenization linked to the building of a macro-element leads,  
588 obviously, to a kind of smoothing of the mechanical heterogeneities related to the  
589 cracking process of a reinforced concrete.
- 590 • The local approach is capable to give detailed information about the cracking process,  
591 it means, microcracks creation accompanying the tortuous propagation of the  
592 macrocrack. It is always an expected result.

593

594 So, now, it is capital to make the comparison related to the computational time linked to the  
595 use of each approach. To do that, it has been chosen to consider only the computational time

596 (average values related to the several simulations performed) related to the crack propagation  
597 in the zone where the rebars are present.

598 This comparison is summarized in Table 4.

599 A look of this Table 4 leads to the following comments:

- 600 • To model the same crack propagation length, the local approach spends ten times  
601 more computational time than the global one.
- 602 • The fact to consider a macro-element with one or two rebars does not lead to a  
603 significant difference concerning the computational time.
- 604 • The fact to model the concrete cracking alone between the cracking of the macro-  
605 elements leads to multiply by two the computational time.

606

607 In fact, to be fully precise, it is important to take into account the simulation time linked to  
608 the numerical tests on tie-beams. If it is done, the total simulation time to perform the 3D  
609 analysis of the DCB specimen is around **26 hours**. It could be considered as too important in  
610 view of the initial objective of this work, it means to propose an approach compatible with  
611 design offices work. But, it should not be forgotten that this simulation time devoted to the  
612 numerical tests replaces real experimental tests which should take more time to be performed.

613

614

## 615 **5. Conclusions and perspectives**

616

617

618 A multi-scale strategy to develop a Probabilistic Model for Elements of Reinforced Concrete  
619 (PMERC) is introduced in this paper. This multi-scale strategy consists in building a macro  
620 model from numerical experimentations using validated local ones: the probabilistic explicit

621 or semi-explicit cracking model for concrete and the interface element model with a Mohr-  
622 Coulomb law for steel/concrete bond.

623 As a validation of this Multi-Scale Modelling Strategy, a previous experimental study related  
624 to the crack propagation in a very large DCB specimen is proposed. The 3D numerical  
625 simulations show that the scientific approach proposed is promising: the global behaviour of  
626 the structure is correctly predicted and the macro-cracking pattern is consistent with results  
627 given by the local approach (only precise information about the tortuosity of the macrocrack  
628 propagation and the microcracks appearance is lost with the macroscopic approach).

629 The main objective of the PMERC is to reduce the massive computational time required to  
630 get information about the cracking process in large structures. It can be considered that this  
631 objective is reached in the considered example. These results could still be improved and the  
632 gain in computational time would be even more acute for larger structures

633 As perspectives go, it is now important to validate the proposed strategy on larger and real-  
634 life structures. It is also necessary to consider the situation where the rebars are positioned in  
635 two or more directions. It is also important to emphasize that the strategy proposed in this  
636 paper, which consists in changing scale of analysis by changing the numerical modelling  
637 scale, can be used in the framework of more sophisticated mechanical models than those  
638 implemented in the present work. For that, it is essential for the local scale models chosen to  
639 have a strong physical relevance and to be fully validated.

640

641

642

643

644

645 **6. Acknowledgement**

646

647

648 The authors gratefully acknowledge the funding support from France's National Research  
649 Agency through the "MACENA" project (ANR-11-RSNR-012).

650

651

652 **7. References**

653

654

- 655 1. Rossi, P., and Richer, S, Numerical modelling of concrete cracking based on a stochastic  
656 approach, *Materials and Structures* 20.5 (1987): 334-337.
- 657 2. Phan, T. S., et al., Numerical modeling of the rebar/concrete interface: case of the flat  
658 steel rebars, *Materials and structures* 46.6 (2013): 1011-1025.
- 659 3. Phan, T. S., Tailhan, J-L and Rossi, P., 3D numerical modelling of concrete structural  
660 element reinforced with ribbed flat steel rebars."Structural Concrete 14.4 (2013): 378-388.
- 661 4. Phan, T. S., Rossi, P. and Tailhan, J-L., Numerical modelling of the concrete/rebar bond,  
662 *Cement and Concrete Composites* 59 (2015): 1-9.
- 663 5. Andriotis, Ch, Gkimousis, I. and Koumousis, V., Modeling Reinforced Concrete  
664 Structures Using Smooth Plasticity and Damage Models, *Journal of Structural*  
665 *Engineering* (2015): 04015105.
- 666 6. Combescure, Ch., Dumontet, H. and Voltaire F., Homogenized constitutive model  
667 coupling damage and debonding for reinforced concrete structures under cyclic  
668 solicitations, *International Journal of Solids and Structures* 50.24 (2013): 3861-3874.

- 669 7. Huguet, M. et al., Homogenized global nonlinear constitutive model for RC panels under  
670 cyclic loadings, *11th World Congress on Computational Mechanics (WCCM XI)*, At  
671 *Barcelona, Spain* (2014).
- 672 8. Sun, B., Xuan W, and Zhaoxia L., Meso-scale image-based modeling of reinforced  
673 concrete and adaptive multi-scale analyses on damage evolution in concrete structures,  
674 *Computational Materials Science* 110 (2015): 39-53.
- 675 9. Oliver, J. et al., Mult-scale (FE<sup>2</sup>) analysis of material failure in cement/aggregate type  
676 composites structures, *Proceedings of EURO-C 2014*, edited by N. Bicanic et al.,  
677 published by CRC Press, pp. 39-49, 2014.
- 678 10. Unger, J.F., Hierarchical multi-scale models for localization phenomena withing the  
679 framework of FE<sup>2</sup>-X<sup>1</sup>, *Proceedings of EURO-C 2014*, edited by N. Bicanic et al.,  
680 published by CRC Press, pp. 75-85, 2014.
- 681 11. Dunn, K. Response Surface Methods, *Process Improvement Using Data*. 250-65, Web.
- 682 12. Bentley, J. L., and Ottmann T. "Algorithms for reporting and counting geometric  
683 intersections." *Computers, IEEE Transactions on* 100.9 (1979): 643-647.
- 684 13. Rossi, P., Wu, X., Probabilistic model for material behaviour analysis and appraisalment  
685 of concrete structures, *Magazine of concrete research* 44.161 (1992): 271-280.
- 686 14. Tailhan, J-L., Dal Pont, S. and Rossi, P., From local to global probabilistic modeling of  
687 concrete cracking, *Annals of Solid and Structural Mechanics* 1.2 (2010): 103-115.
- 688 15. Rossi, P., et al., Scale effect on concrete in tension, *Materials and Structures* 27.8 (1994):  
689 437-444.
- 690 16. Rossi, P., Ulm, F-J, Hachi, F., Compressive behaviour of concrete: physical mechanisms  
691 and modeling, *Journal of Engineering Mechanics* 122.11 (1996): 1038-1043.
- 692 17. Lemaitre, J., Chaboche, J.L., *Mechanics of solid materials*. Cambridge University press,  
693 Cambridge, 1994.

- 694 18. Rossi, P., Tailhan, J.L., Cracking of concrete structures: interest and advantages of the  
695 probabilistic approaches. *In: Rilem international conference on numerical modelling*  
696 *strategies for sustainable concrete structures, SSCS'2012. Aix-en-Provence, France,*  
697 2012.
- 698 19. Jirasek, M., Zimmermann, T., Rotating crack model with transition to scalar damage. *J*  
699 *Eng Mech* 124(3):277–284, 1998.
- 700 20. Rots, J.G., Nauta, P., Kuster, G.M.A., Blaauwendraad, J., Smeared crack approach and  
701 fracture localization in concrete, *HERON* 30(1), 1985.
- 702 21. De Borst, R., Nauta, P., Non-orthogonal cracks in a smeared finite element model. *Eng*  
703 *Comput* 2(1):35–46, 1985.
- 704 22. Jirasek, M., Damage and smeared crack models. *In: Hofstetter G, Meschke G (ed)*  
705 *Numerical modeling of concrete Ann. Solid Struct. Mech. cracking. CISM International*  
706 *Centre for Mechanical Sciences, vol 532. Springer, Vienna, pp 1–49, 2011.*
- 707 23. Meschke, G., Grasberger, S., Becker, C., Jox, S., Numerical modeling of concrete  
708 cracking. *Springer, chap Smeared Crack and X-FEM Models in the Context of*  
709 *poromechanics, pp 265–327, 2011.*
- 710 24. Bazant, Z., Oh, B., Crack band theory for fracture of concrete. *Mater struct* 16(3):155–  
711 177, 1983.
- 712 25. Feller, W., An introduction to probability theory and its applications, *vol 2. Wiley, New*  
713 *York, 2008.*
- 714 26. Irwin, G., Linear fracture mechanics, fracture transition, and fracture control. *Eng Fract*  
715 *Mech* 1(2):241–257, 1968.
- 716 27. Rossi, P., Comportement dynamique des bétons: du matériau à la structure. *Annales de*  
717 *l'Institut technique du bâtiment et des travaux publics. No. 511. Institut technique du*  
718 *bâtiment et des travaux publics, 1993 5 (in french).*



- 719 28. Lundgren K., Bond between ribbed bars and concrete. Part 1: Modified model, *Magazine*  
720 *of Concrete Research*, 57 (7) (2005): 371-382.
- 721 29. Rossi, P., Fissuration du béton : du matériau à la structure. Application de la mécanique  
722 linéaire de la rupture. PhD Thesis, Ecole Nationale des Ponts et Chaussées, p. 228, 1986  
723 (in french), published in *rapport de recherche des LPC*, n°150, 1988 (in french).
- 724 30. Rossi, P., Coussy, O., Boulay, C., Acker, P., Comparison between plain concrete  
725 toughness and steel fibre reinforced concrete toughness, *Cement and Concrete Research*,  
726 vol. 16, pp. 303-313, 1986.
- 727 31. Rossi, P., Coupling between the crack propagation velocity and the vapour diffusion in  
728 concrete. *Materials and Structures*, vol. 22, pp. 91-97, 1989.
- 729

730

## **List of tables**

731

732 Table 1. Model parameters values related to the concrete (semi-explicit approach) and the  
733 steel behaviours in the framework of the local 2D approach (tie-beams simulations).

734 Table 2. Model parameters values related to the 3D macroscopic approach

735 Table 3. Model parameters values related to the 2D concrete/steel bond behavior (2D  
736 simulations)

737 Table 4. Computational times related to the crack propagation in the zone where the rebars  
738 are present (for 2D and 3D numerical modellings)

739

740

**Tables**

741 Table 1

Material	Parameter	Value	Unit
<b>Concrete</b>	<b>Tensile strength (Weibull distribution)</b>		MPa
	Scale parameter	8.0	
	Shape parameter	1.0	
	<b>dissipated energy <math>G_c</math> (lognormal distribution)</b>		
	Mean value	1.3	$10^{-4}\text{MN mm}^{-2}$
	Deviation	8.4	$10^{-4}\text{MN mm}^{-2}$
	<b>Compressive strength</b>	55	MPa
	<b>Young modulus</b>	35000	MPa
<b>Steel</b>	<b>Young modulus</b>	191000	MPa
	<b>Elastic limit</b>	400	MPa

742

743

744 Table 2

745

ERC Type	Parameter	Symbol	Value (MPa)
<b>ERC5</b>	Tensile strength	$\sigma_t^{cri}$	
	Mean	$\mu_{\sigma_t^{cri}}$	3.2
	Deviaion	$\sigma_{\sigma_t^{cri}}$	0.4
	Tensile recovery	$\sigma_r$	1.3
	Residual stiffness	$E'_1$	
	Mean	$\mu_{E'_1}$	1000.
	Deviation	$\sigma_{E'_1}$	50.
<b>ERC10</b>	Tensile strength	$\sigma_t^{cri}$	
	Mean	$\mu_{\sigma_t^{cri}}$	3.05
	Deviaion	$\sigma_{\sigma_t^{cri}}$	0.4
	Tensile recovery	$\sigma_r$	0.75
	Residual stiffness	$E'_1$	
	Mean	$\mu_{E'_1}$	390.
	Deviation	$\sigma_{E'_1}$	50.
<b>ERC20</b>	Tensile strength	$\sigma_t^{cri}$	
	Mean	$\mu_{\sigma_t^{cri}}$	3.4
	Deviaion	$\sigma_{\sigma_t^{cri}}$	0.6
	Tensile recovery	$\sigma_r$	0.75
	Residual stiffness	$E'_1$	
	Mean	$\mu_{E'_1}$	550.
	Deviation	$\sigma_{E'_1}$	100.

746

747  $\mu_{\sigma_t^{cri}}, \sigma_{\sigma_t^{cri}}$ , are the parameters of the lognormal distribution function of the tensile strength,

748 and  $\mu_{E'_1}, \sigma_{E'_1}$ , are the parameters of the lognormal distribution function of the residual

749 stiffness after cracking.

750

751

752

753

754

755

756 Table 3

<b>Cohesion</b>	<b><math>C</math></b>	10	<b><math>MPa</math></b>
<b>Critical tangent displacement</b>	<b><math>\delta_t^{cri}</math></b>	4	<b><math>10^{-6}m</math></b>

757

758

759 Table 4

<b>Model used</b>	<b>Calculation time (sec)</b>	<b>Number of elements in the reinforced zone</b>	<b>Number of nodes in the reinforced zone</b>
Local	4750	2318	1398
Macro-ERC1	527	1125	1480
Macro-ERC2	1220	2057	2592
Macro-ERC3	520	625	888

760

## List of figures

761

762

763 Fig.1. Probabilistic concrete cracking model – explicit approach

764 Fig.2. Probabilistic concrete cracking model – semi-explicit approach

765 Fig.3. steel-concrete interface behaviour law

766 Fig.4. Macroscopic model

767 Fig.5. DCB dimensions and loading conditions

768 Fig.6. Position of the rebars in the DCB specimen.

769 Fig.7. Example of 3D finite element mesh of the DCB specimen (ERC1)

770 Fig.8. 2D cuts of the 3D finite element meshes of the DCB specimen related to the three ERC

771 Fig.9. 2D finite element meshes of the three numerical tie-beams

772 Fig.10. Example of cracking process obtained with TB1

773 Fig.11. Example of cracking process obtained with TB2

774 Fig.12. Example of cracking process obtained with TB3

775 Fig.13. Three 3D finite elements meshes related to the three numerical tie-beams  
776 (macroscopic approach)

777 Fig.14. Load-Displacement curves related to the macroscopic and local modellings of TB1

778 Fig.15. Load-Displacement curves related to the macroscopic and local modellings of TB2

779 Fig.16. Load-Displacement curves related to the macroscopic and local modellings of TB3

780 Fig.17. Crack mouth opening displacement (CMOD) versus loading curves (DCB specimen)  
781 related to ERC1

782 Fig.18. Crack mouth opening displacement (CMOD) versus loading curves (DCB specimen)  
783 related to ERC2

784 Fig.19. Crack mouth opening displacement (CMOD) versus loading curves (DCB specimen)  
785 related to ERC3

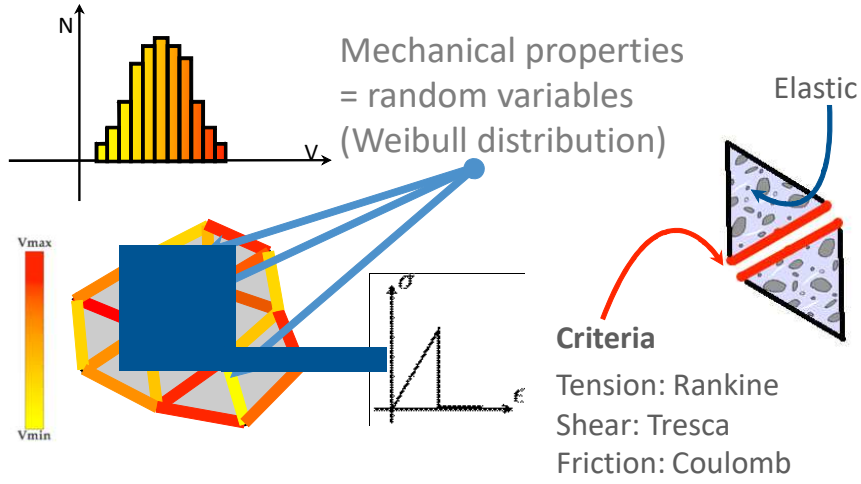
786 Fig.20. Example of cracking pattern of the DCB specimen obtained with 3D simulations –  
787 Macroscopic model

788 Fig.21. 2D Finite elements mesh related to the local approach

789 Fig.22. Crack mouth opening displacement (CMOD) versus loading (DCB specimen) related  
790 to the local approach

791 Fig.23. Example of cracking pattern of the DCB specimen obtained with 2D simulations –  
792  
793

**Figures**

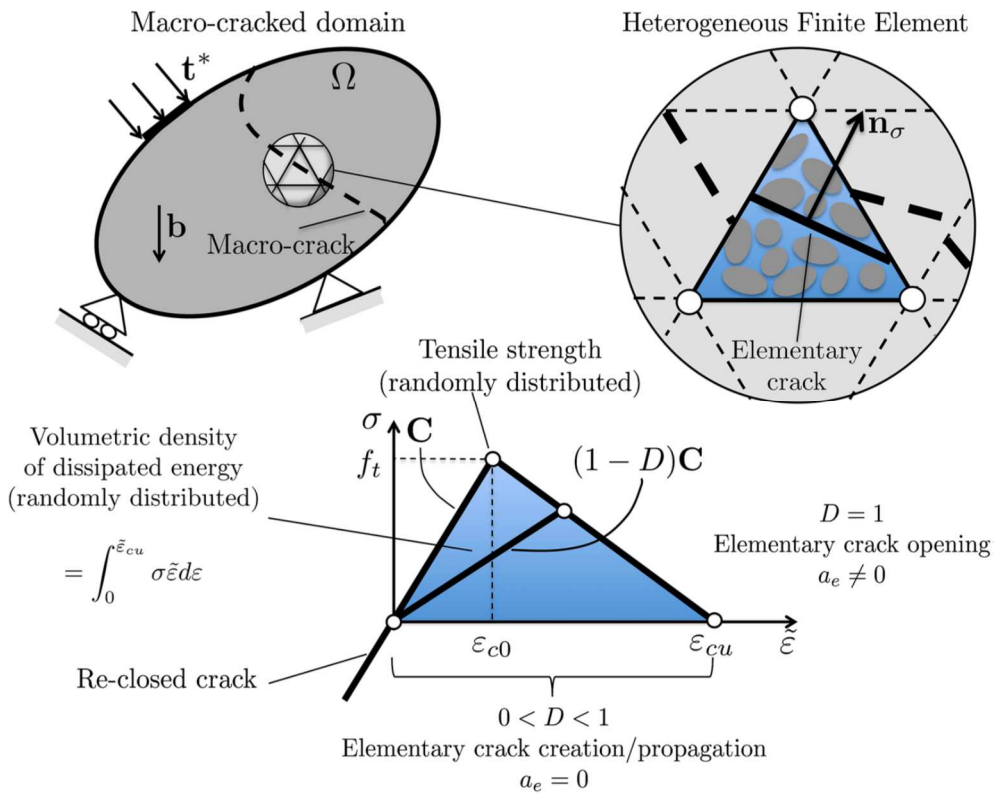


795

796

Fig.1

797



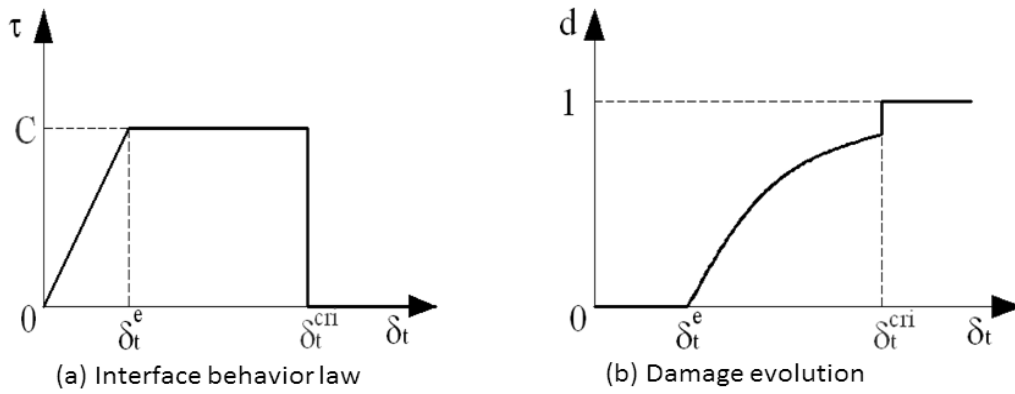
798

799

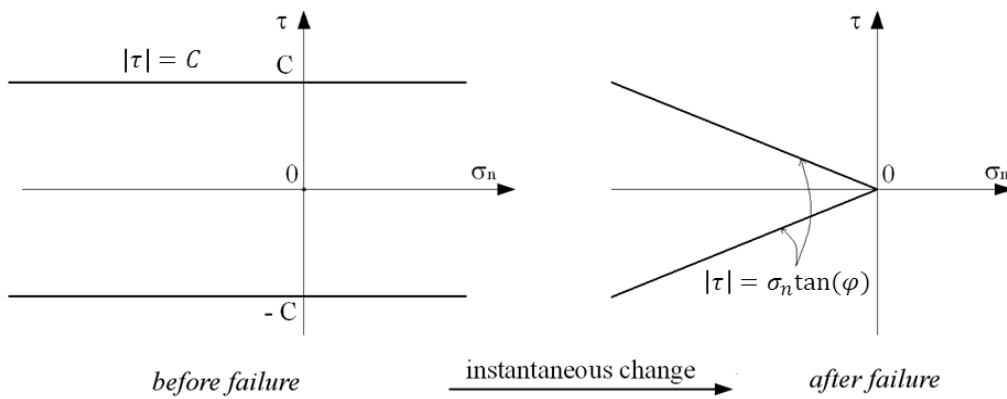
Fig. 2



800



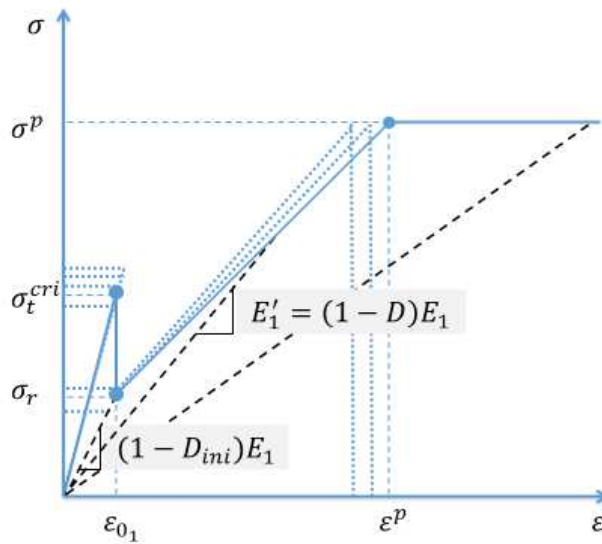
801



802

803

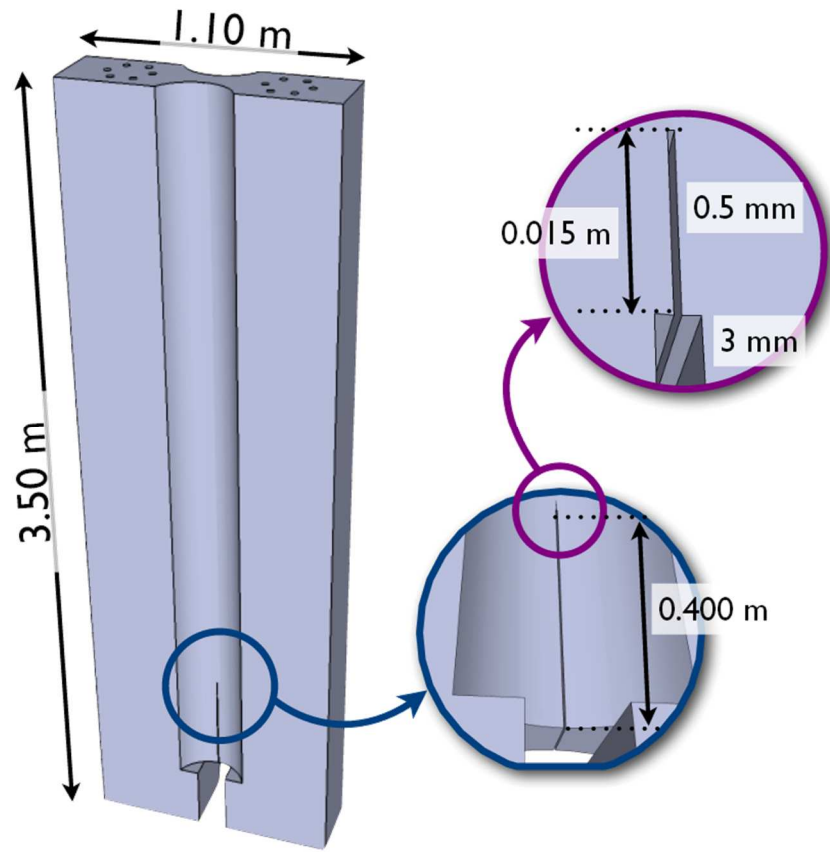
Fig.3



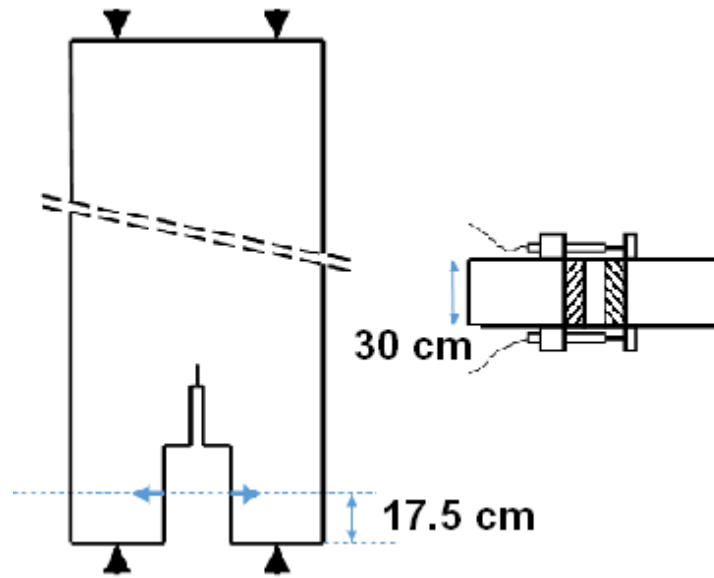
804

805

Fig.4



806



807

808

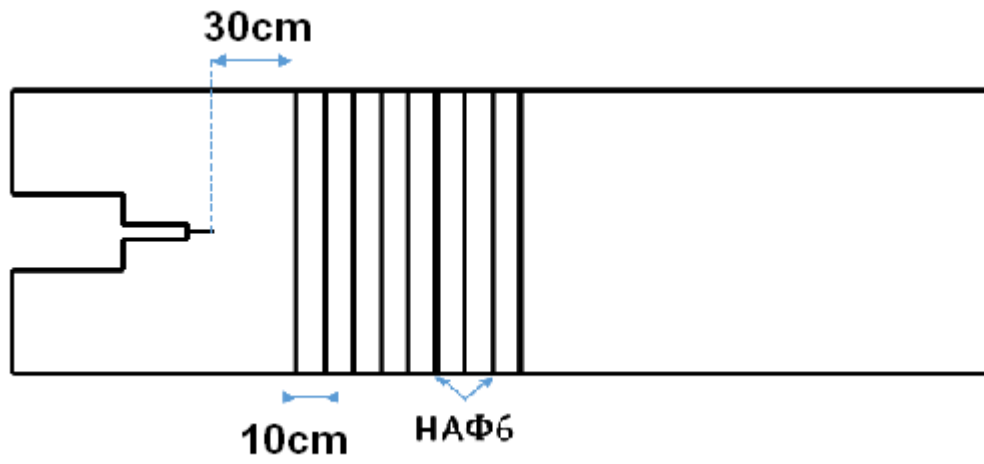
809

810

811

812

Fig.5

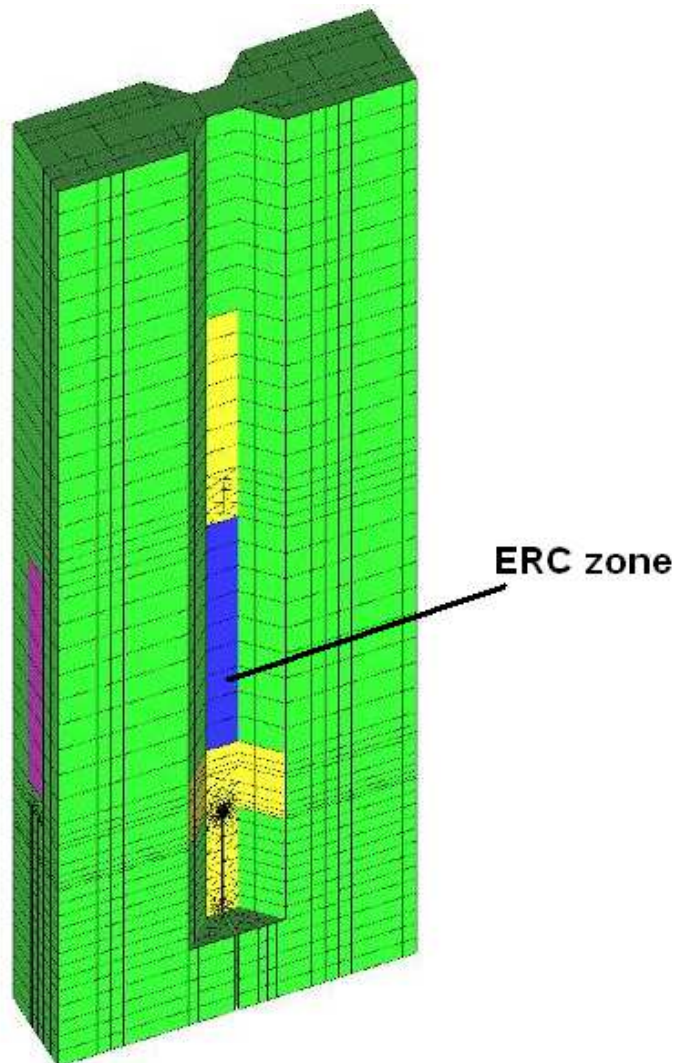


813

814

Fig.6

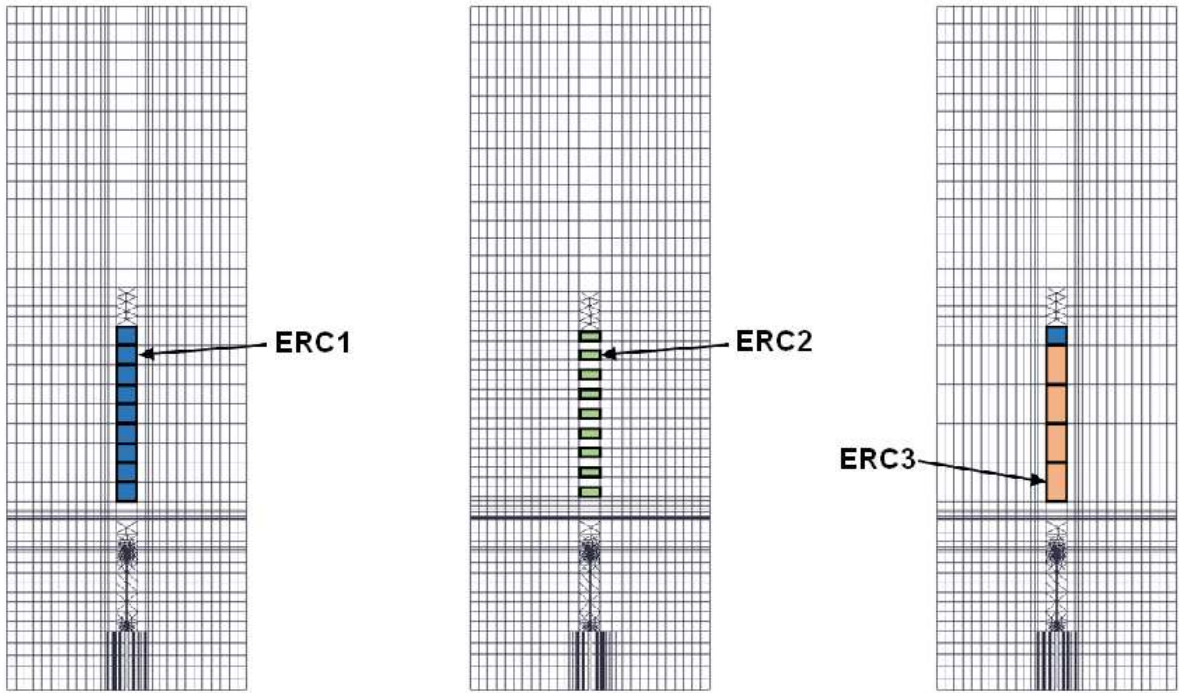
815



816

817

Fig.7

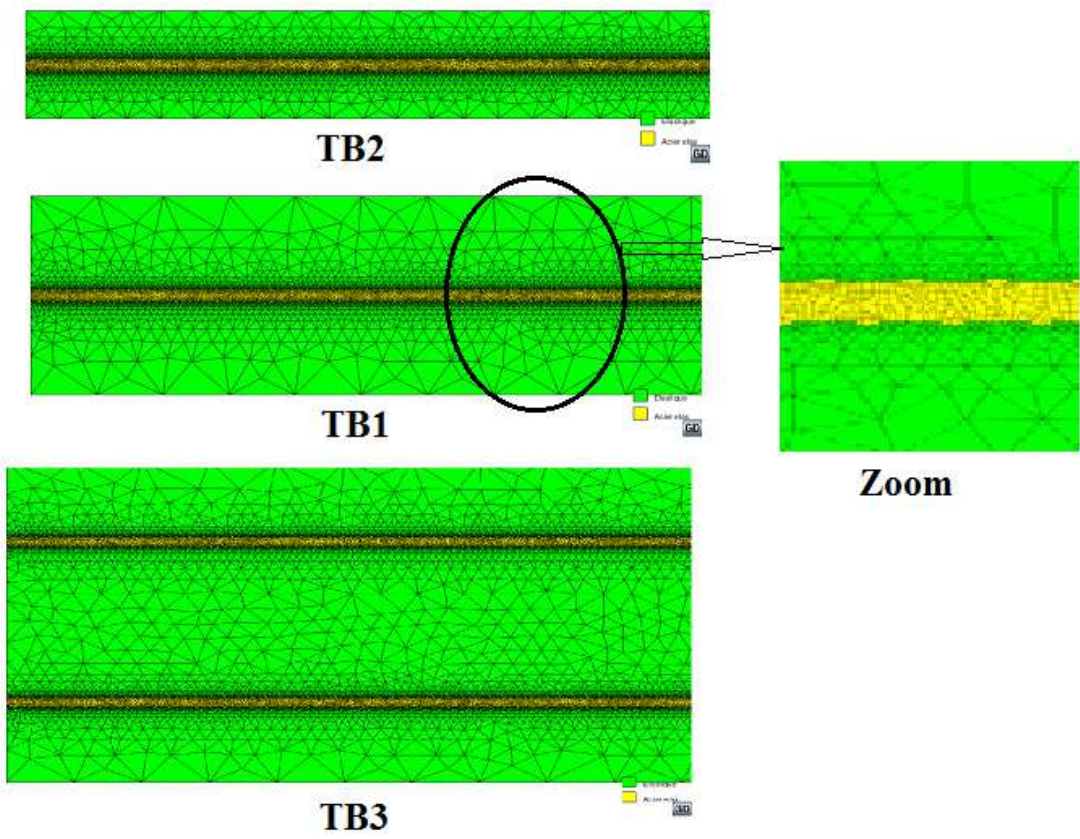


818

819

820

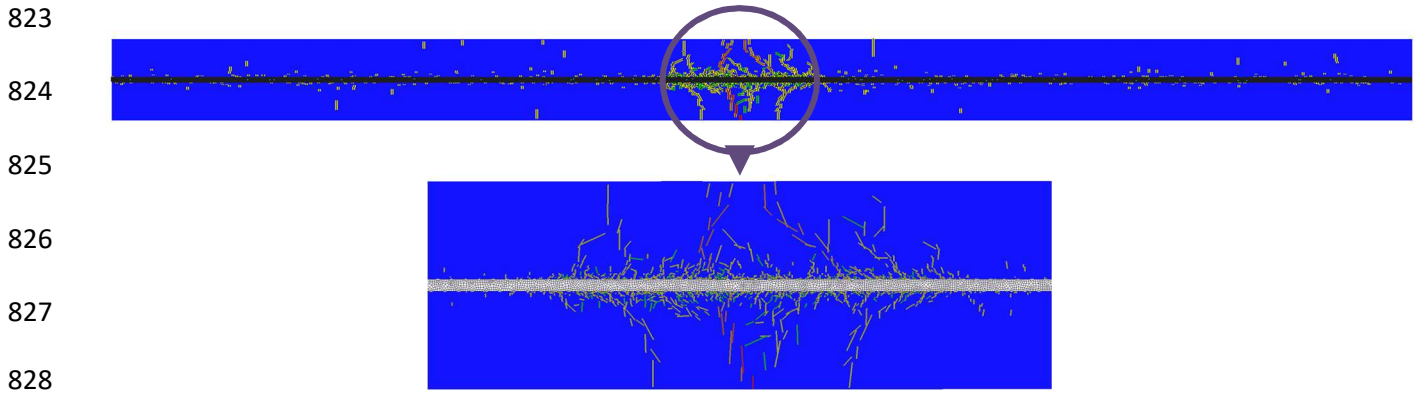
Fig. 8



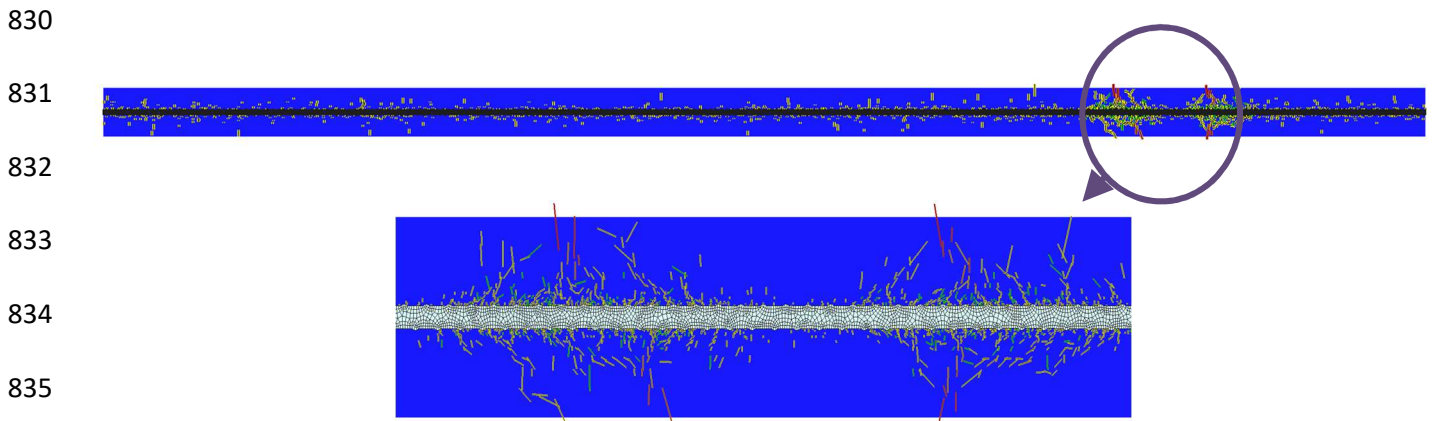
821

822

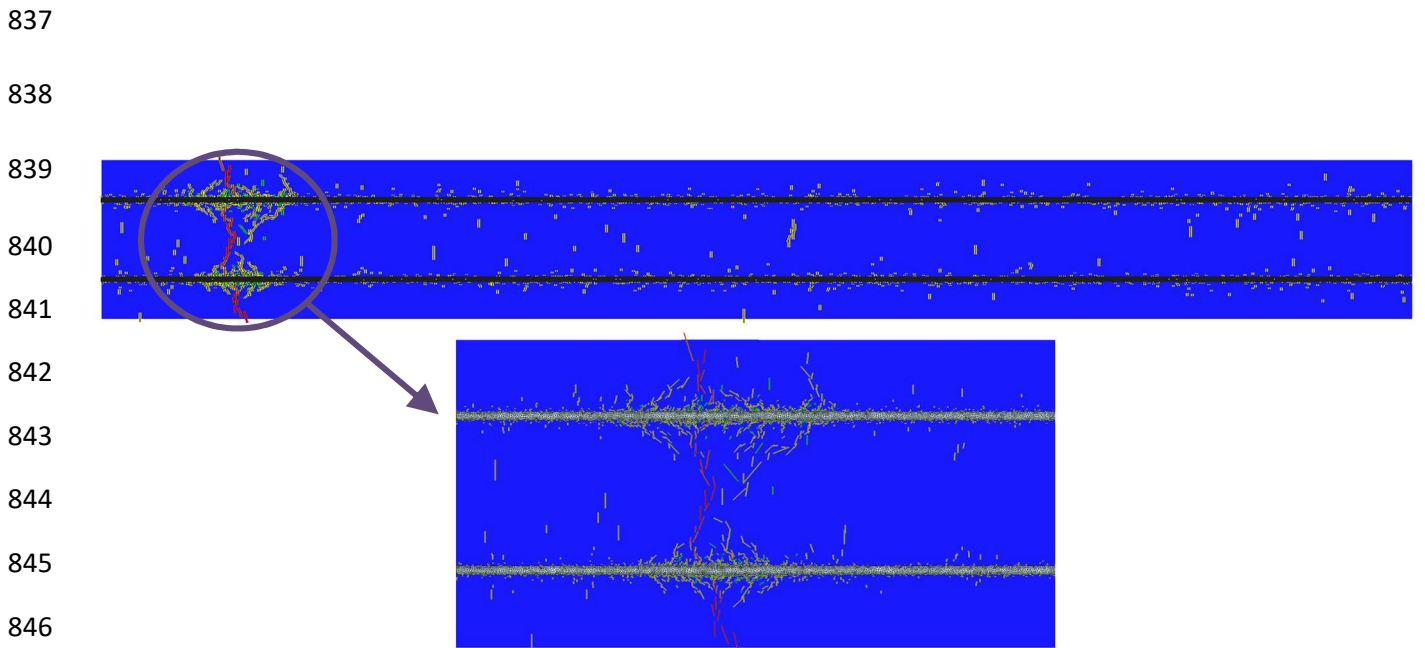
Fig.9



829 Fig. 10

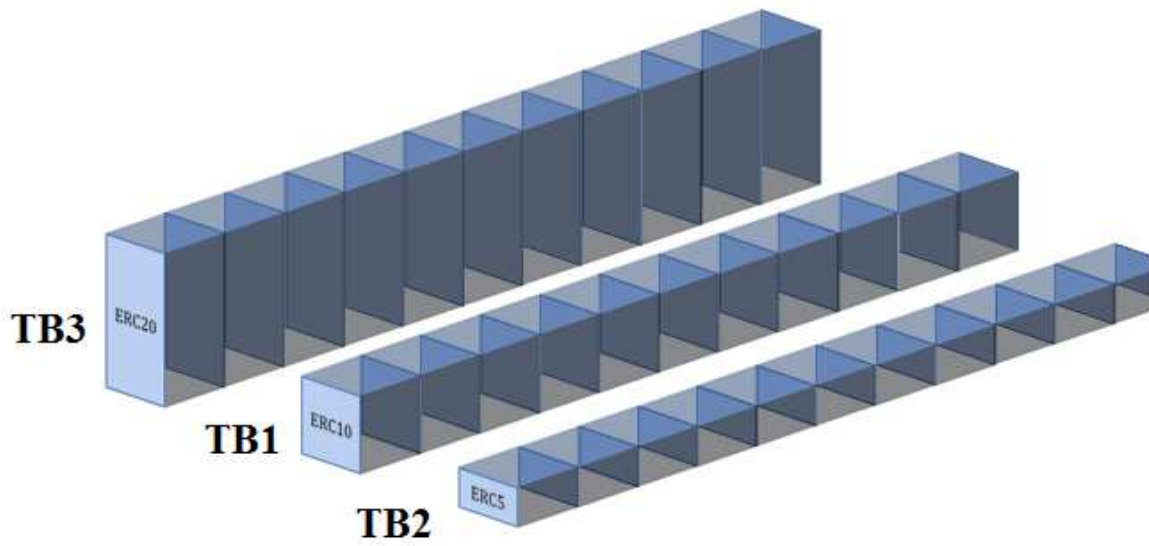


836 Fig.11



847 Fig.12



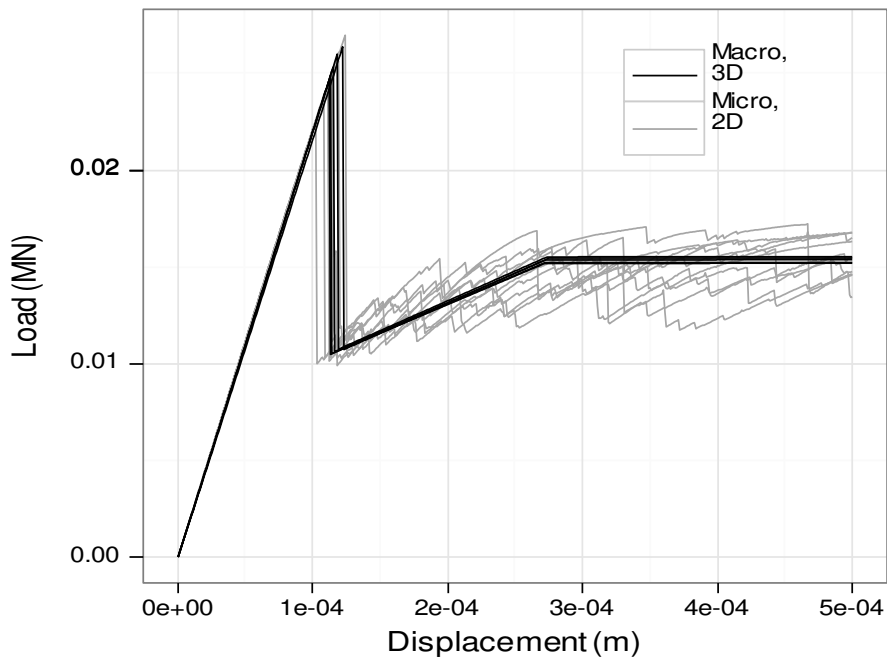


850

851

852

Fig.13



853

854

855

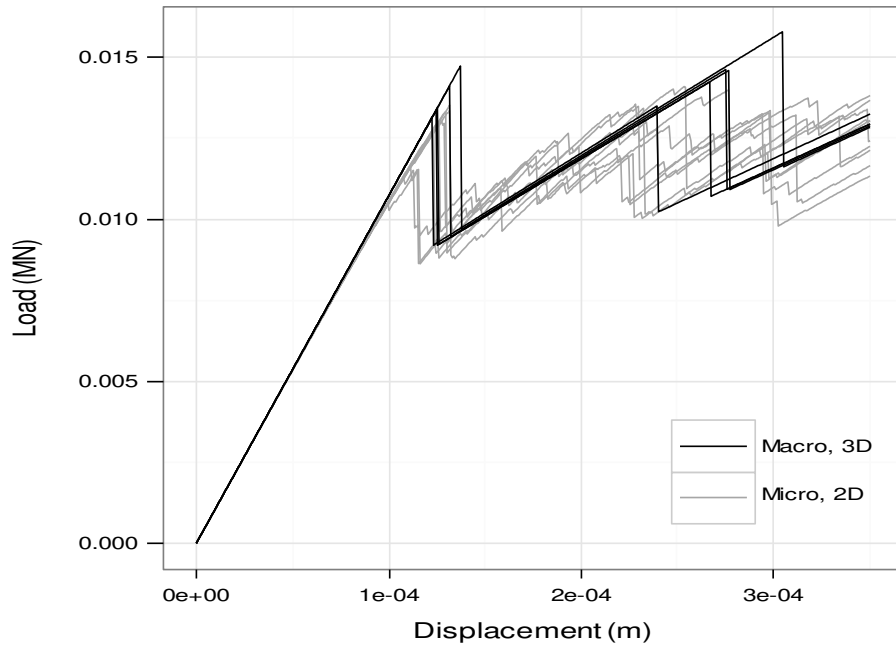
856

857

858

859

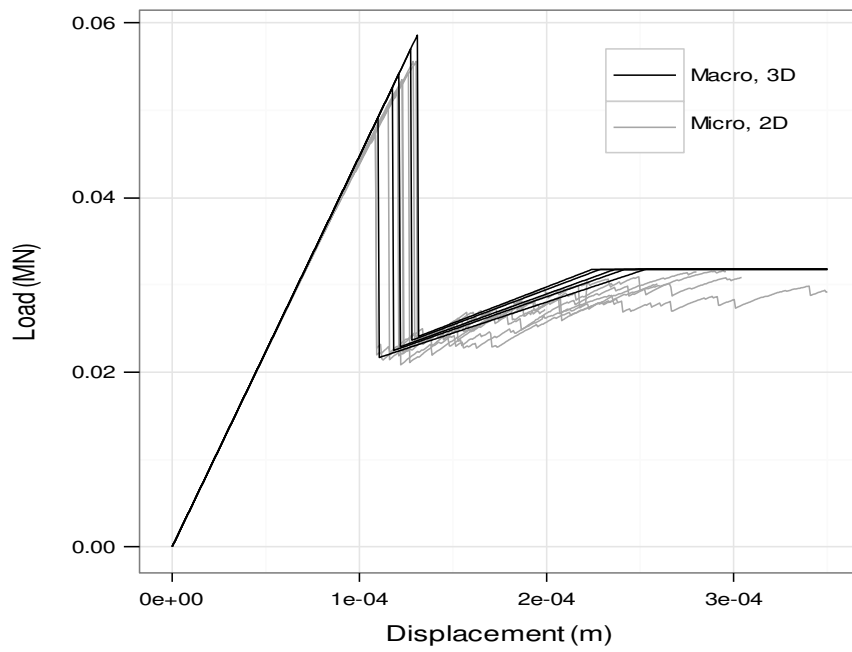
Fig. 14



860

861

Fig. 15

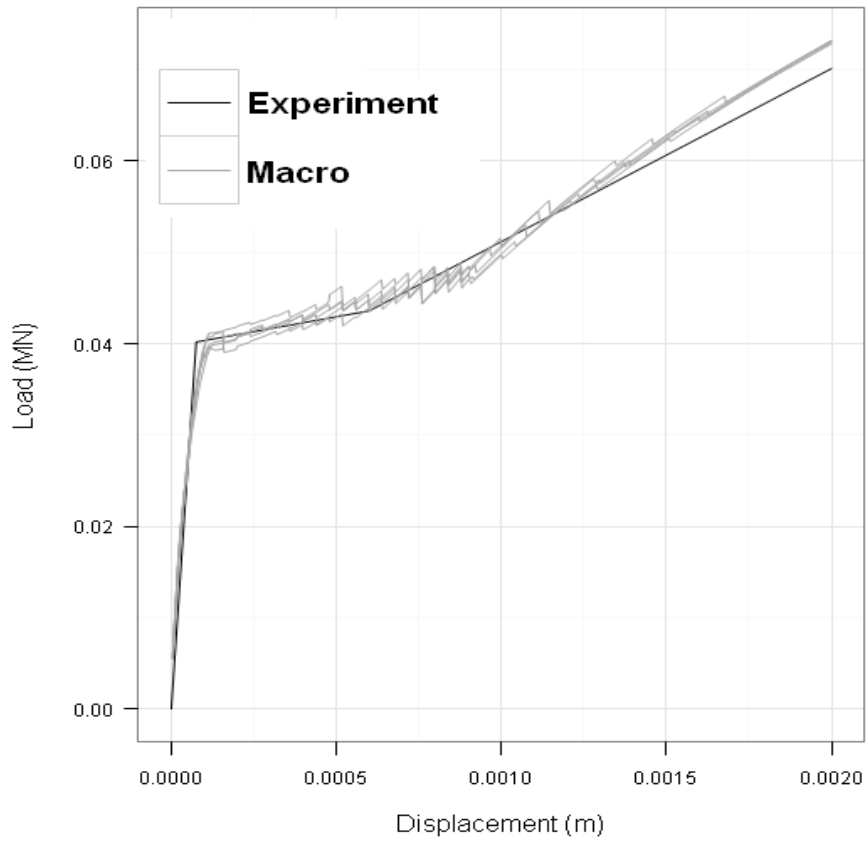


862

863

864

Fig. 16

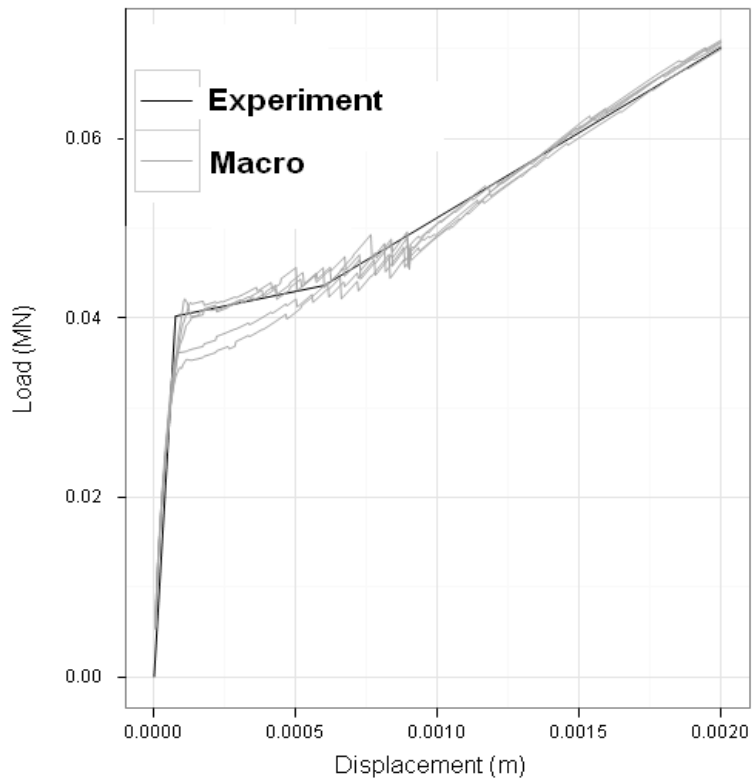


865

866

Fig. 17

867

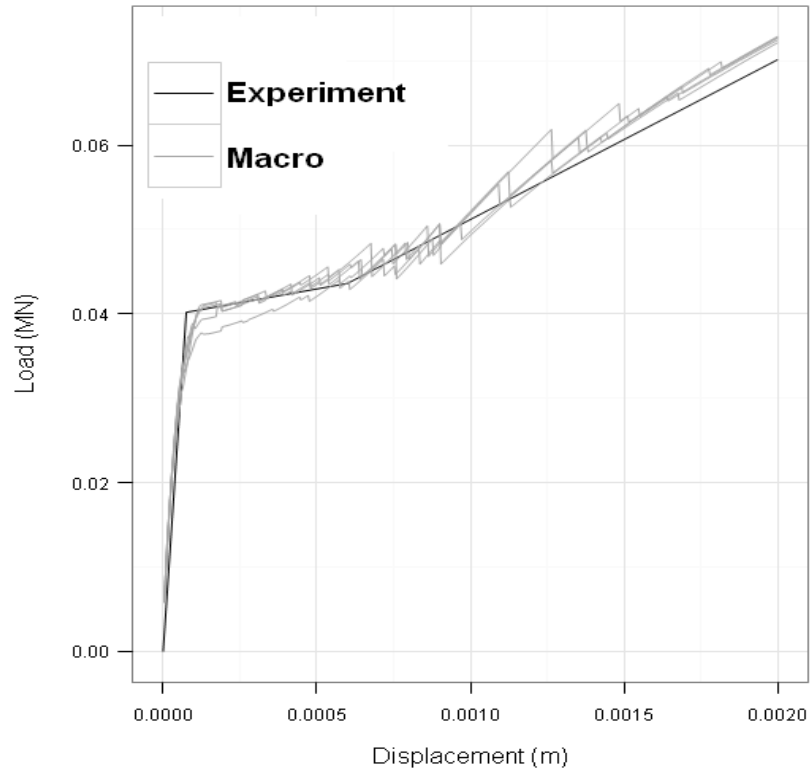


868

869

Fig. 18



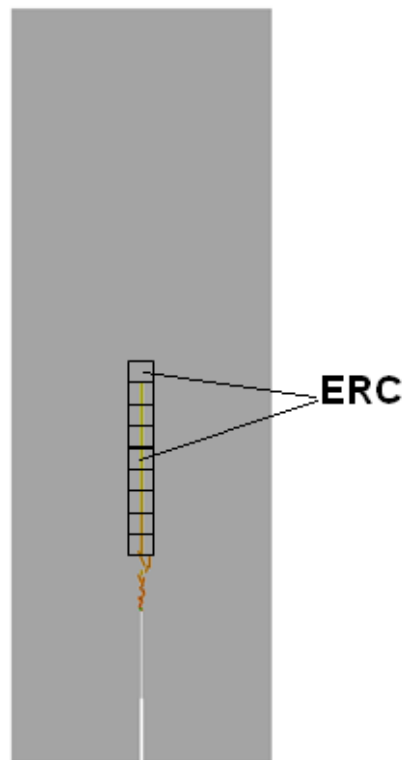


870

871

872

Fig. 19



873

874

Fig. 20

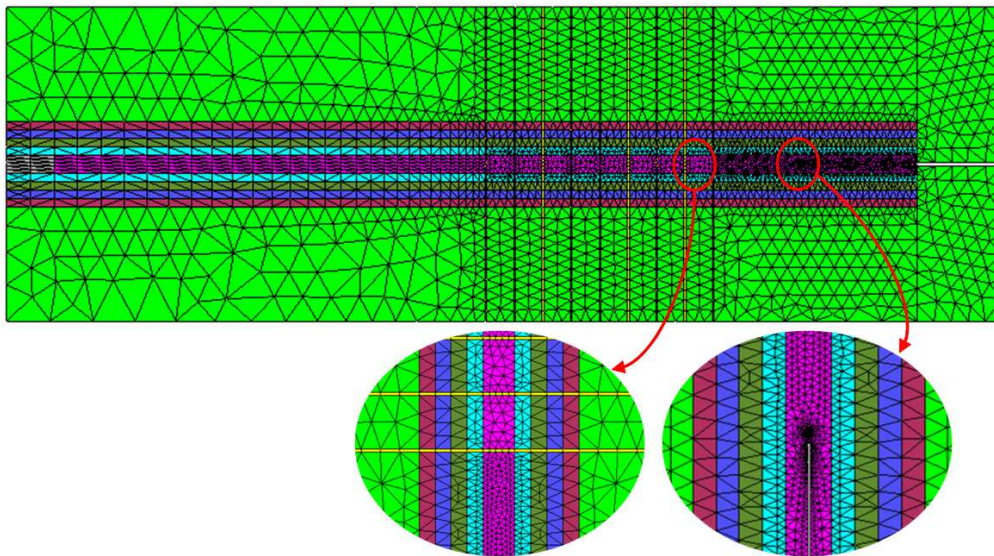


Fig. 21

875

876

877

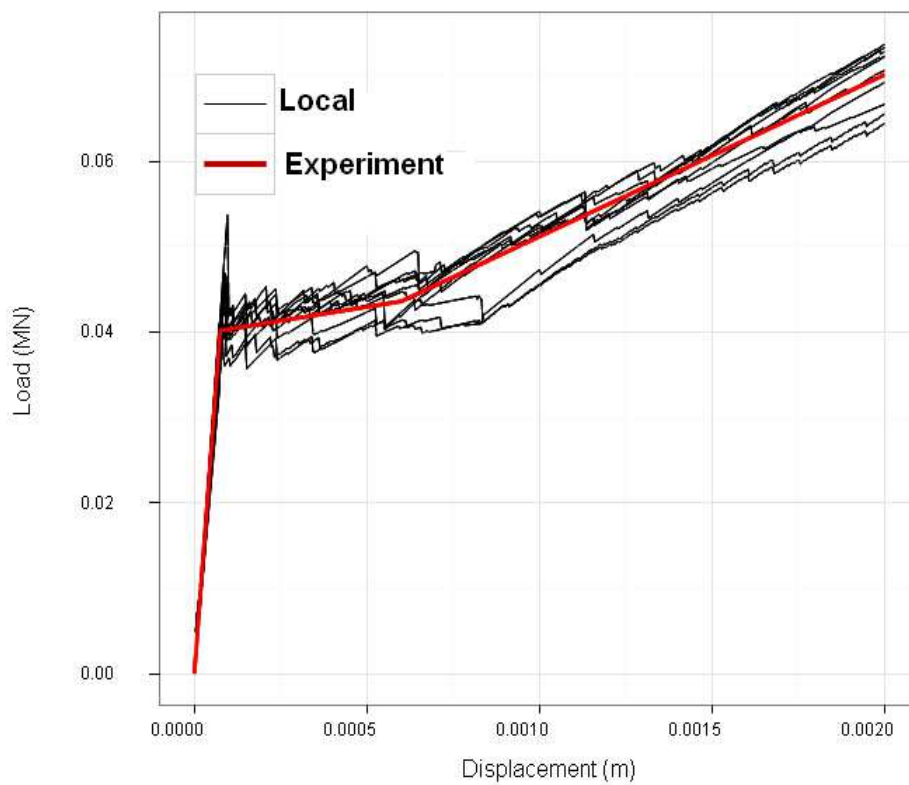


Fig. 22

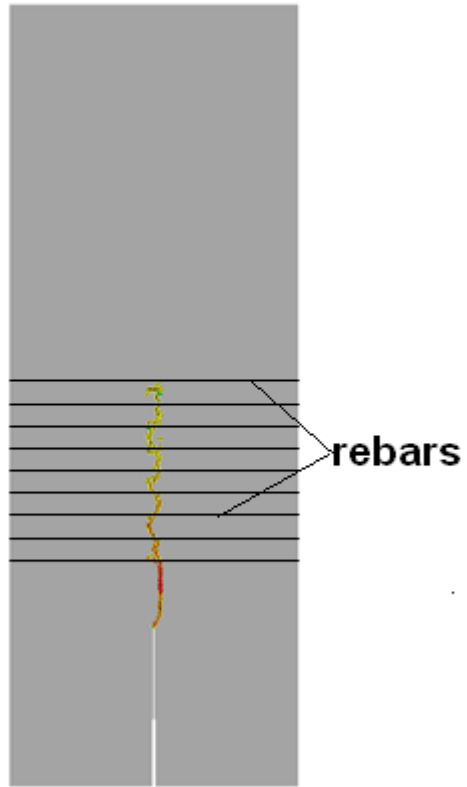
878

879

880

881

882



883

884

Fig.23